Supplementary Information for

"An alternative route to single ion conductivity using multi-ionic salts"

Sumanth Chereddy[1], Parameswara Rao Chinnam[1]*, Vijay Chatare[1], Stephen Patrick diLuzio[1], Mallory P. Gobet[2], Steven G. Greenbaum[2], and Stephanie L. Wunder[1]*
[1]Department of Chemistry, Temple University, Philadelphia, PA 19122
[2]Department of Physics, Hunter College, CUNY, New York, NY 10065
*slwunder@temple.edu; chprbhu@temple.edu

Table of Contents

Experimental

Materials:

Bis(trifluoromethane) sulfonamide lithium salt (LiTFSI) and tetraglyme (G_4) (Sigma Aldrich) were dried at 60°C in vacuuo, and G_4 further dried over molecular sieves in an argon purged glove box. Lithium metal (Alfa-Aesar) was stored in a desiccator inside an argon purged glove box. Octasilane POSS (SH1310) was a gift from Hybrid Plastics, Inc. and used as received. All the starting materials for synthesis of the salt were purchased from Sigma-Aldrich and used as received. Carbon coated $LiFePO_4$ was purchased from Ximen Tob New Energy Technology Co. Ltd. Carbon black, PVDF binder and 2-NMP were purchased from MTI Corporation.

Synthesis of POSS-($LiNSO_2CF_3$)$_8$:

Synthesis of POSS-($LiNSO_2CF_3$)$_8$ = $Si_8O_8[(Si(CH_3)_2–R)]_8$ with R = $–CH_2CH_2CH_2NLiSO_2CF_3$ is presented in Scheme 1. The details of the synthesis of allyltrifluoromethylsulfonamide (1), the hydrosilyation of allyltrifluoromethylsulfonamide with octasilane POSS to form $Si_8O_8[(Si(CH_3)_2–R)]_8$, R = $–CH_2CH_2CH_2NHSO_2CF_3$ (2), and the conversion to the lithium salt (3), and their characterization can be found in Thesis reference[1]

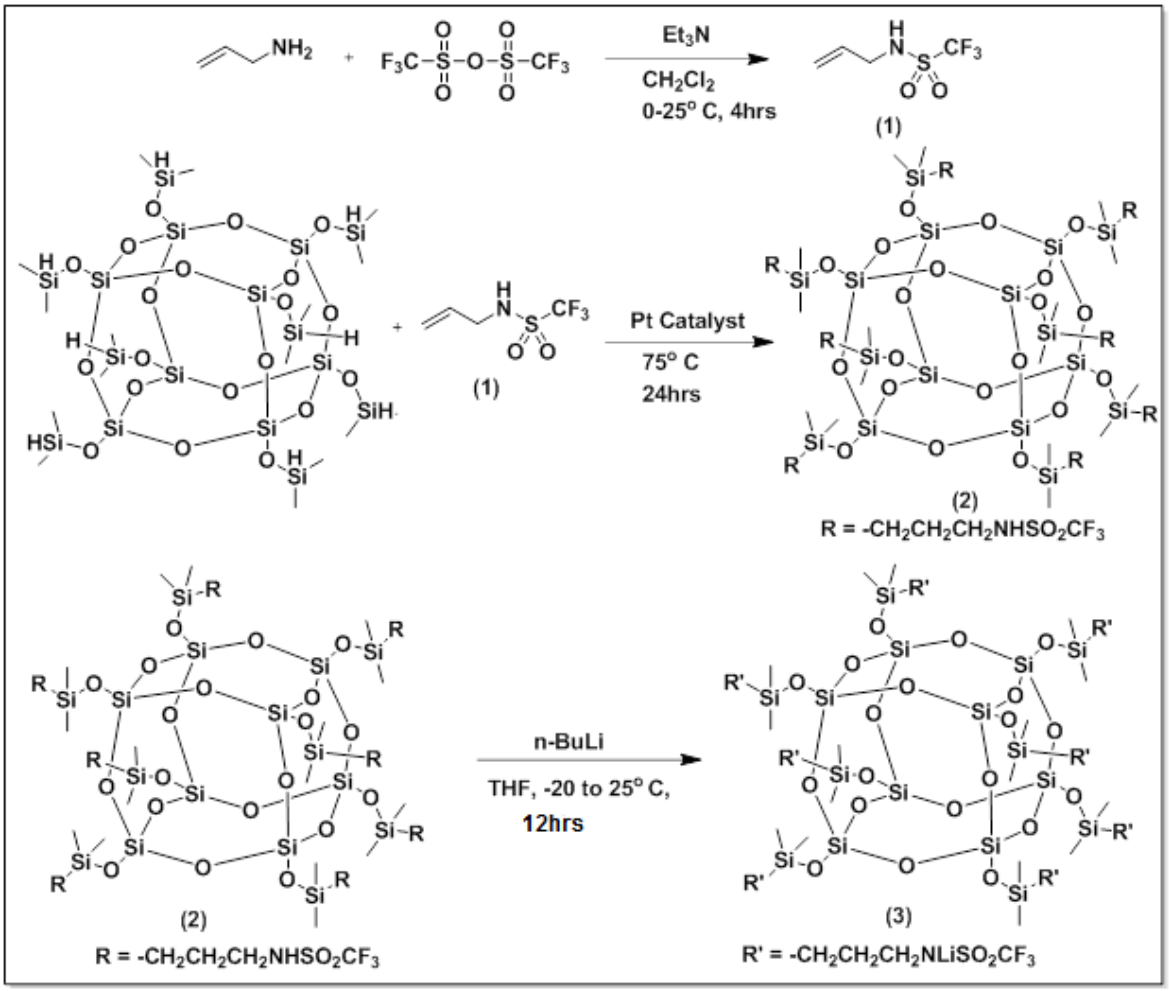

Scheme S1. Reaction scheme to form multi-ionic lithium salt POSS-($LiNSO_2CF_3$)$_8$

Electrolyte Preparation:

Electrolytes were prepared by adding calculated amounts of G_4, POSS-$(LiNSO_2CF_3)_8$ and/or LiTFSI together in an argon purged MBraun glove box and stirred overnight at room temperature (RT). The compositions are given in **Table S1**.

Table S1. Sample Compositions

			LiTFSI			POSS-$(LiNSO_2CF_3)_8$		
O/Li	G_4 g	G_4 moles x 10^{-4}	g	moles x 10^{-4}	moles G_4 / moles LiTFSI	g	moles 10^{-4}	moles G_4 / moles POSS
20/1	0.150	6.75	0.048	1.67	4/1	0.054	0.2096	32/1
17.5/1	0.150	6.75	0.055	1.91	3.5/1	0.062	0.2406	28/1
15/1	0.150	6.75	0.064	2.22	3.0/1	0.072	0.2795	24/1
12.5/1	0.150	6.75	0.077	2.68	2.5/1	0.087	0.3377	20/1
10/1	0.150	6.75	0.097	3.37	2.0/1	0.1088	0.4223	16/1
7.5/1	0.150	6.75	0.129	4.49	1.5/1	0.1448	0.5621	12/1
1.5/1	0.150	6.75	0.194	6.75	1/1	0.217	0.8423	8/1
2.5	0.150	6.75	0.387	13.4	0.5	0.434	1.68	4/1
								wt% LiTFSI /wt% POSS-$(LiNSO_2CF_3)_8$
19.3/1	0.150	6.75	0.00216	0.075		0.054	0.2096	04/96
16.4/1	0.150	6.75	0.0108	0.376		0.054	0.2096	20/80
15/1	0.150	6.75	0.0162	0.564		0.054	0.2096	30/70
18.5/1	0.150	6.75	0.048	1.67		0.0048	0.0186	90/10
17.1	0.150	6.75	0.048	1.67		0.0096	0.0372	80/20
8.6/1	0.150	6.75	0.077	3.46		0.015	0.0582	80/20
16/1	0.150	6.75	0.048	1.67		0.0144	0.0559	70/30
9.7/1	0.150	6.75	0.064	2.88		0.0192	0.0745	70/30
Molecular weights: G_4 222.28 g/mol; LiTFSI 287.1g/mol; POSS-$(LiNSO_2CF_3)_8$ 2576 g/mol								

Experimental

Characterization: SAXS, TEM DSC, TGA, PFG-NMR

Small angle scattering data (SAXS) were obtained on an Anton Paar SAXSpoint 2.0 system with 50 W Primux microfocus source, Montel optics with 99.9% spectral purity, 2 x 2 pairs of scatterless single crystal slits, and a Dectris Eiger R 1M detector. TEM data were obtained on an FEI Technai 12T electron microscope with operating voltage of 120 KeV. Differential scanning calorimetry (DSC) was obtained on a TA Instruments Hi-Res DSC 2920 at 10°C min^{-1} under N_2. Except as noted, samples were scanned from 25°C to 100°C, 100°C to -100°C and -100°C to 100°C, with the second heating scans reported. The glass transition temperature, T_g, was taken as the midpoint of the heat capacity (Cp) versus temperature plots. Thermogravimetric analysis (TGA) data was obtained on a TA Instruments 2950, scanned from 25 to 800° C at a rate of 10° C min^{-1} under N_2. Viscosity (η) of the electrolytes was measured in a B cell (η range 2000 cP) in a Rheosense m-VROC viscometer. The NMR experiments were done with a 400 SB Bruker Avance III spectrometer at 25°C. Self-diffusion experiments were done using a PFG stimulated-echo sequence with bipolar gradient pulses, 2 spoiler gradients, and a 5 ms longitudinal eddy-current delay (LED).

Electrochemical Measurements:

For all electrochemical measurements, the electrolytes were soaked in Whatman glass fiber separators. Separators with large pores such as Celgard and the even larger 1.6 mm pores of glass fiber filters (Whatman) used in this investigation.

Ionic conductivities were measured by AC impedance spectroscopy using a Gamry potentiostat/galvanostat/ZRA (model interface 1000) in the frequency range from 1 Hz to 1 MHz. Control of the equipment was through Gamry framework software and data was analyzed with Gamry Echem analysis software. The AC perturbation voltage was 10 mV. Temperature dependent conductivities were obtained in a homemade electrochemical cell (1 cm^2 stainless steel blocking electrodes) that was thermostatted in the oven of a cryogenic liquid N_2 gas chromatograph (GC). The electrochemical cell was placed in the oven of the GC and annealed overnight at 90°C. Conductivity measurements were made on the cooling cycle and heating cycles (the resistances on the heating and cooling cycles were very close) and the heating cycles are reported. At each temperature above RT, the sample was equilibrated for about 30 minutes. Conductivities, σ (mS cm^{-1}), were obtained using $\sigma = (t/AR)$, where t is the separator thickness in cm, A is the separator cross-sectional area in cm^2 and R is the bulk resistance in mΩ.

Interfacial resistance, lithium plating-stripping and lithium ion transport numbers (t_{Li}^+) were obtained using the appropriate electrolyte with symmetric non-blocking lithium electrodes at 25°C. The interfacial resistance was measured under open circuit potential as a function of time. The lithium ion transference number was obtained using the modified d.c./a.c., steady-state current method, which contains corrections for slow diffusion coefficients of the ionic species, slow electrode kinetics and passivation films formed on the electrodes[2-4]: $t_{Li}^+ = I_{ss}(\Delta V - I_o R_o)/I_o(\Delta V - I_s R_{ss})$ or the same but multiplied by R_{ss}/R_o (however, here $R_{ss} \sim R_o$). A DC pulse (ΔV) of 20 mV was used to polarize the cell, and the initial current, I_o, and resistance, R_o and final, steady state, I_{ss}, R_{ss} values measured. I_o originates from the migration of both the

anions and cations, while I_{ss} is due to the migration of only the cations. Data was fit to the appropriate equivalent circuits using Echem analysis software.

Half-cell testing, using an Arbin BT-G generation battery tester, was obtained for Li/(G_4/POSS-(LiNSO2CF3)8 O/Li = 20/1)/$LiFePO_4$, Li/(G_4/LiTFSI O/Li = 20/1)/$LiFePO_4$ and Li/(G_4/POSS-(LiNSO2CF3)8 O/Li = 20/1)/$LiFePO_4$ in CR 2032 coin cells,. A glass fiber separator (Whatman glass microfiber filters, Grade GF/A) soaked with the G_4/POSS-(LiNSO2CF3)8 O/Li = 20/1 electrolyte was used. Li^0 metal was used as the counter and reference electrodes. The cathode was made with $LiFePO_4$/carbon black/PVDF binder (8/1/1) using N-methyl-2-pyrrolidone (NMP) to form a slurry (~ 1.9-2.2 mg/cm^2 $LiFePO_4$) that was doctor-bladed onto battery grade aluminum foil to make 50 micron thick electrodes. The electrodes were dried in a vacuum oven overnight at 120°C. The dried electrodes were rolled with a Durston flat agile F130 mm rolling mill mechanical presser to make good contact between the electrode and the current collector. The assembled cells were kept at 60°C overnight to wet the cathode with the viscous electrolytes. All the battery testing was at 25°C between 2.6 and 4.0V. The current range of the cells was taken based on the theoretical capacity of 170mAh/g for Li/$LiFePO_4$.

Table S2 σ and t_+^{PP} of G_4/LiX/POSS-$(LiNSO_2CF_3)_8$ as a function of composition

LiX/POSS-$(LiNSO_2CF_3)_8$ wt%	X	O/Li	σ S/cm 30 ^{0}C	σ S/cm 90 ^{0}C	t_+^{pp}
100/0	PF_6^-				0.52, 0.49
100/0	BETI$^-$				0.49, 0.57
100/0	TFSI$^-$	20/1	5.0 x 10^{-3}	14.3 x 10^{-3}	0.47, 0.46, 0.44
100/0	TFSI$^-$	17.5/1	4.9 x 10^{-3}	15.0 x 10^{-3}	
90/10	TFSI$^-$	18.5/1	4.0 x 10^{-3}	9.1 x 10^{-3}	0.60, 0.63
80/20	TFSI$^-$	17.1	3.3 x 10^{-3}	7.9 x 10^{-3}	0.71, 0.69, 0.73
80/20	PF_6^-				0.65, 0.67
80/20	BETI$^-$				0.66, 0.69
70/30	TFSI$^-$	16/1	3.5 x 10^{-3}	8.2 × 10^{-3}	0.61
70/30	TFSI$^-$	9.7/1	3.0 x 10^{-3}	9.6 x 10^{-3}	0.65, 0.67
30/70	TFSI$^-$	19.6	9.3 x 10^{-4}	2.9 x 10^{-3}	0.64, 0.65
20/80	TFSI$^-$	16.4/1	1.0 x 10^{-3}	3.0 x 10^{-3}	0.63, 0.64
04/96	TFSI$^-$	19.3/1	3.5 x 10^{-4}	9.2 x 10^{-4}	
0/100	TFSI$^-$	17.5/1	2.3 x 10^{-4}	6.4 x 10^{-4}	
0/100	TFSI$^-$	20/1	2.5 x 10^{-4}	6.7 x 10^{-4}	0.65, 0.67, 0.69

*****Since samples were prepared by weight ratios of LiTFSI/POSS-$(LiNSO_2CF_3)_8$, the O/Li are not all the same; however, conductivities of samples between O/Li = 10/1 to 20/1 do not change much.

Table S3. Viscosity of G_4, G_4/LiTFSI and G_4/POSS-$(LiNSO_2CF_3)_8$ as function of temperature			
T (^{0}C)	Viscosity (mPa·s) of tetraglyme (G_4), and G_4 + salts with O/Li = 20/1		
	G_4	G_4/LiTFSI	G_4/POSS-$(LiNSO_2CF_3)_8$
10	3.7	20.7	23.7
30	3.0	10.3*	14.8
50	2.0	5.7	8.2
70	1.5	3.6	5.0
*Comparable data previously reported[5]			

Table S4. Glass transition (T_gs) and melt (T_m) temperatures and enthalpies (ΔH_m) for G_4/Li salts									
	G_4/POSS-$(LiNSO_2CF_3)_8$					G_4/LiTFSI			
O/Li	moles G_4 / moles POSS	T_g ^{0}C	T_m ^{0}C	ΔH_m* J/g		moles G_4 / moles LiTFSI	T_g ^{0}C	T_m ^{0}C	ΔH_m^* J/g
100/0 (G_4)			-28.3	126.8				-28.3	126.8
20/1	32/1	-78	-32.1	91		4/1	-98	-46.9	55
17.5	28/1	-76	-32.9	85		3.5	-94	-42.9	7
15/1	24/1	-79	-34.5	78		3/1	-91	-	-
12.5	20/1	-76	-36.5	70		2.5/1	-87	-	-
10/1	16/1	-92	-38.8	36~		2/1	-83	-	-
7.5/1	12/1	-85	N/A	N/A		1.5/1	-76	-	-
5/1	8/1	-74	N/A	N/A		1/1	-57	-	-
2.5/1	4/1	-64	N/A	N/A		0.5/1	-38	-	-
Mixed G_4/LiTFSI/POSS-$(LiNSO_2CF_3)_8$									
	wt%POSS-$(LiNSO_2CF_3)_8$/ wt%LiTFSI								
19.3/1	04/96								
16.4/1	20/80	-81	-36.3	69					
15/1	30/70	-91	-40.2	44					
18.5/1	90/10	-97	-46	47					
17.1/1	80/20	-97	-47	36					

16/1	70/30	-95	-49	29					
9.7/1	70/30	-90	N/A	N/A					
*ΔH_m is normalized for the amount of G_4									

TEM Images

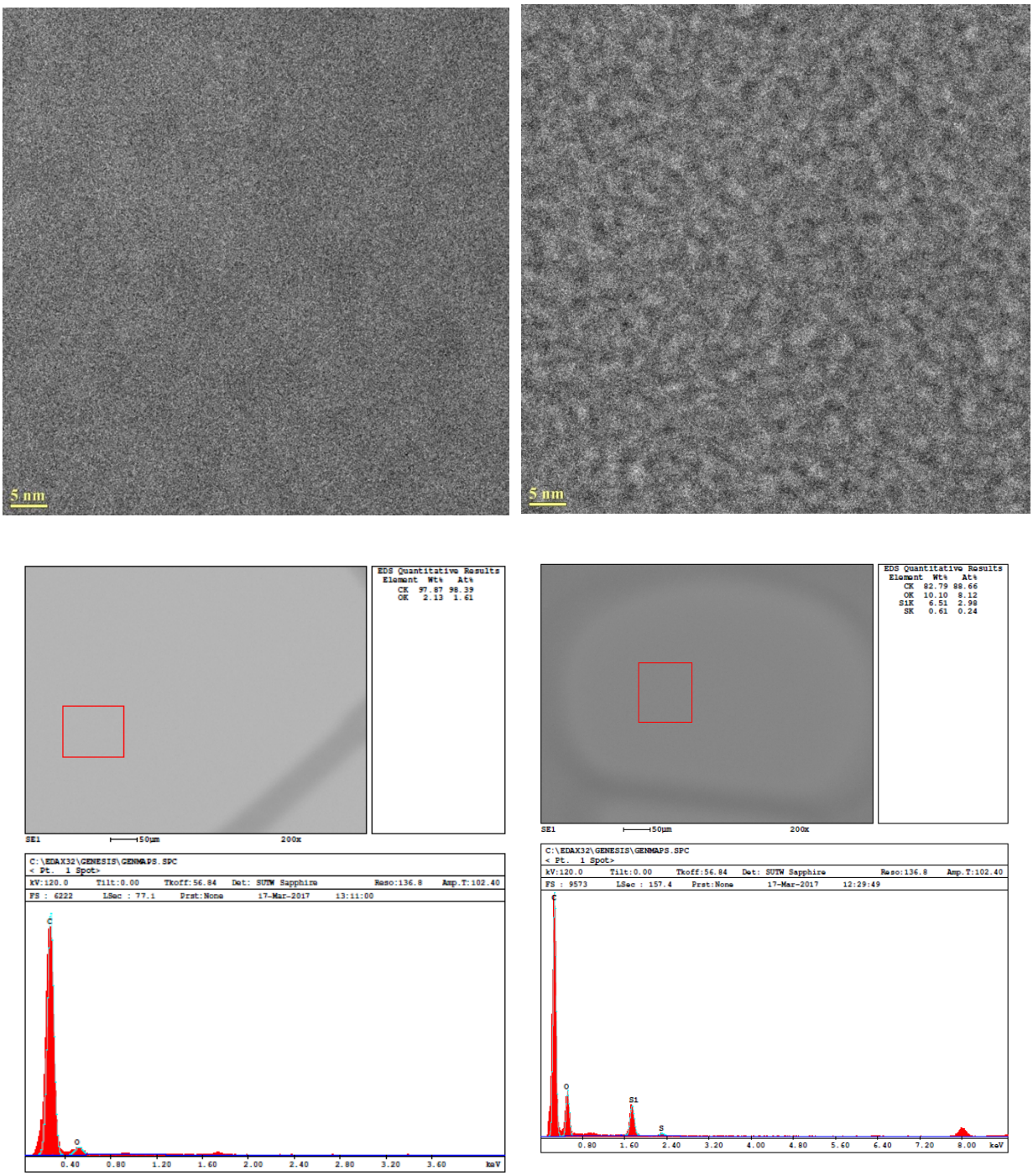

Figure S 1A. TEM images of empty grid and grid with G_4/POSS-$(LiNSO_2CF_3)_8$, 1/1 molar ratio (O/Li = 5/1), polymerized in PEGMEA, with EDAX showing Si on sample.

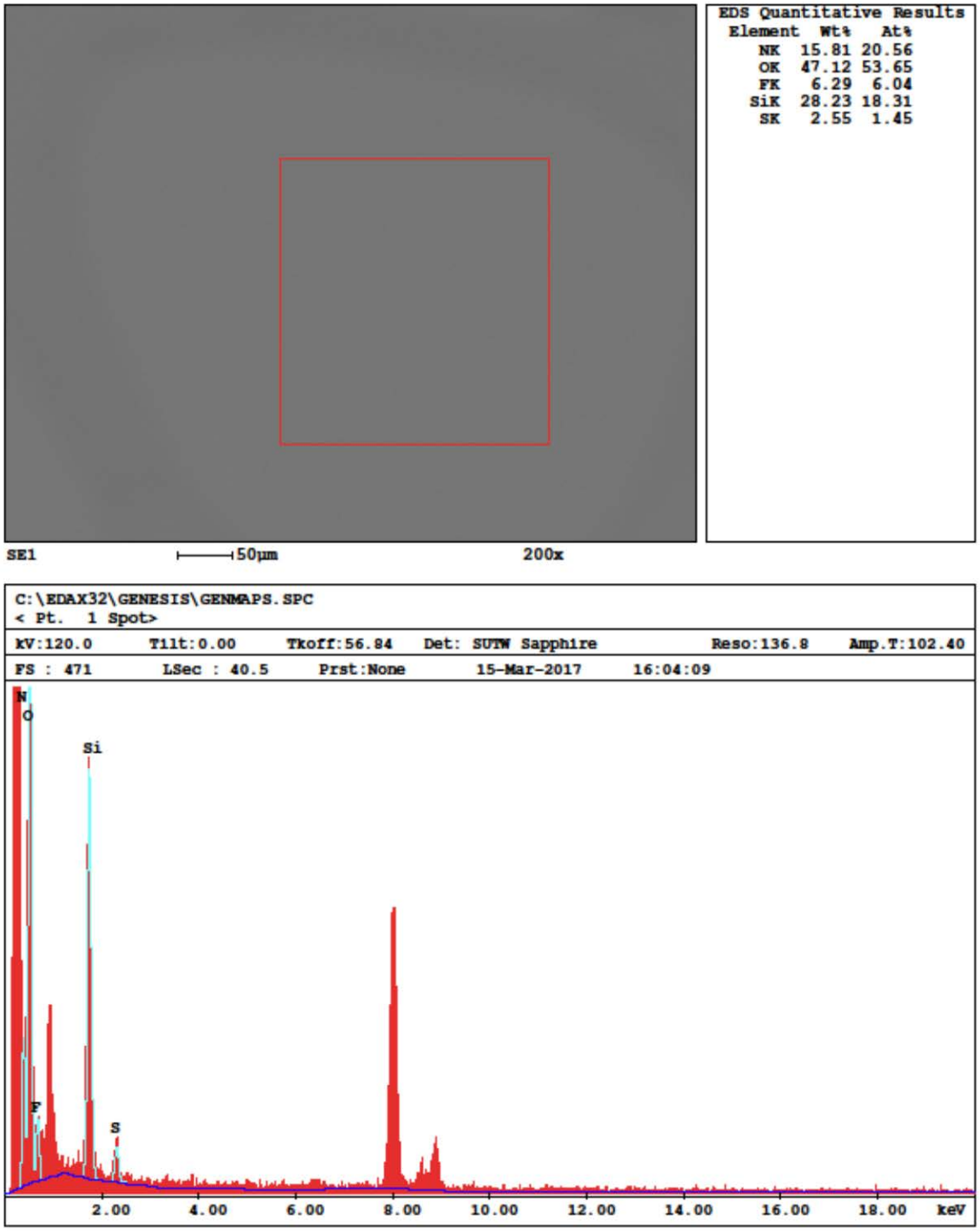

Figure S1B. TEM image on larger spot size of G_4/POSS-$(LiNSO_2CF_3)_8$, 1/1 molar ratio (O/Li = 4/1), polymerized in PEGMEA, with EDAX showing Si, F, S and O on sample.

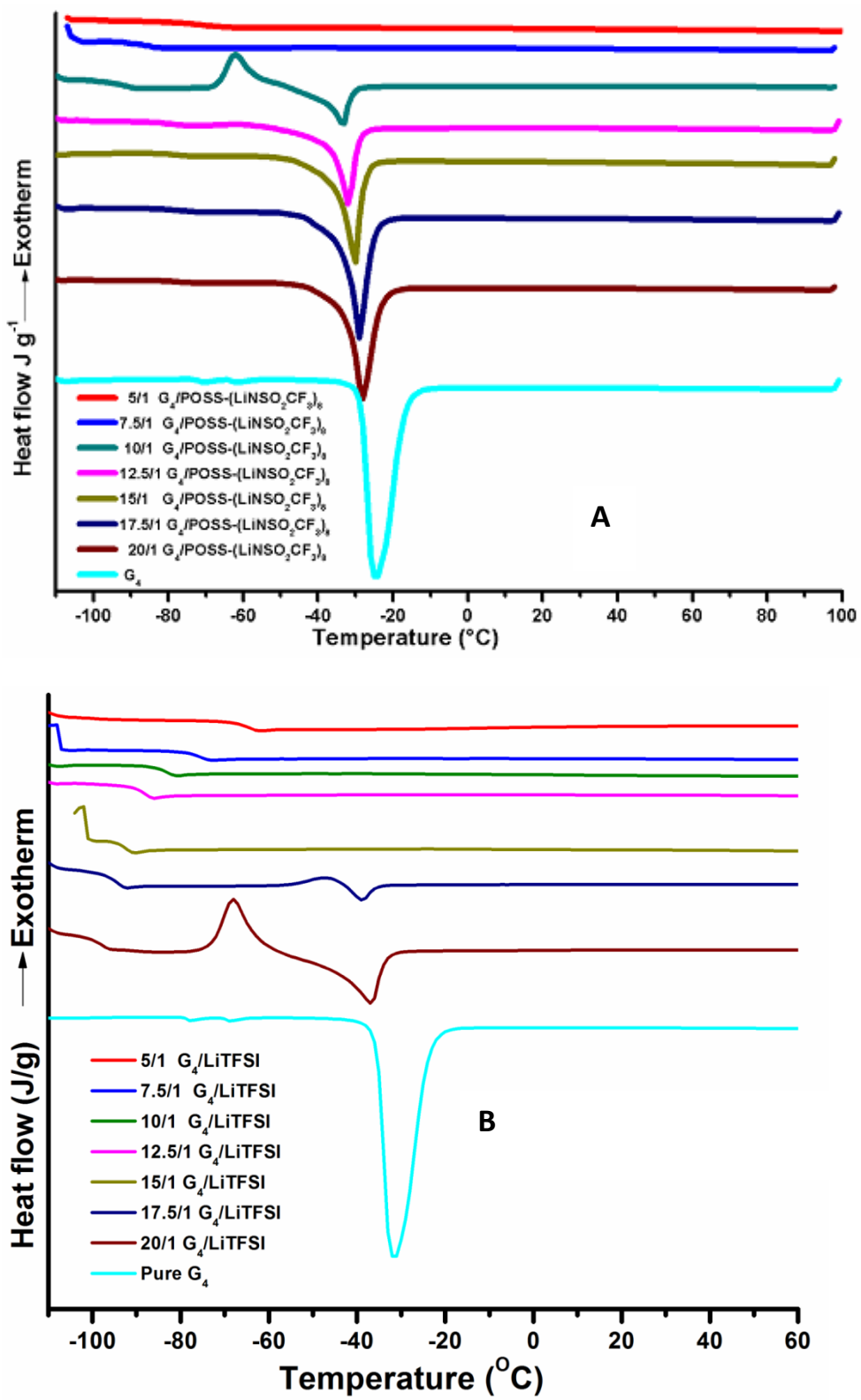

Figure S2. DSC thermograms for second heating cycles of (**A**) G_4/POSS-$(LiNSO_2CF_3)_8$ and (**B**) G_4/LiTFSI, both at different O/Li ratios

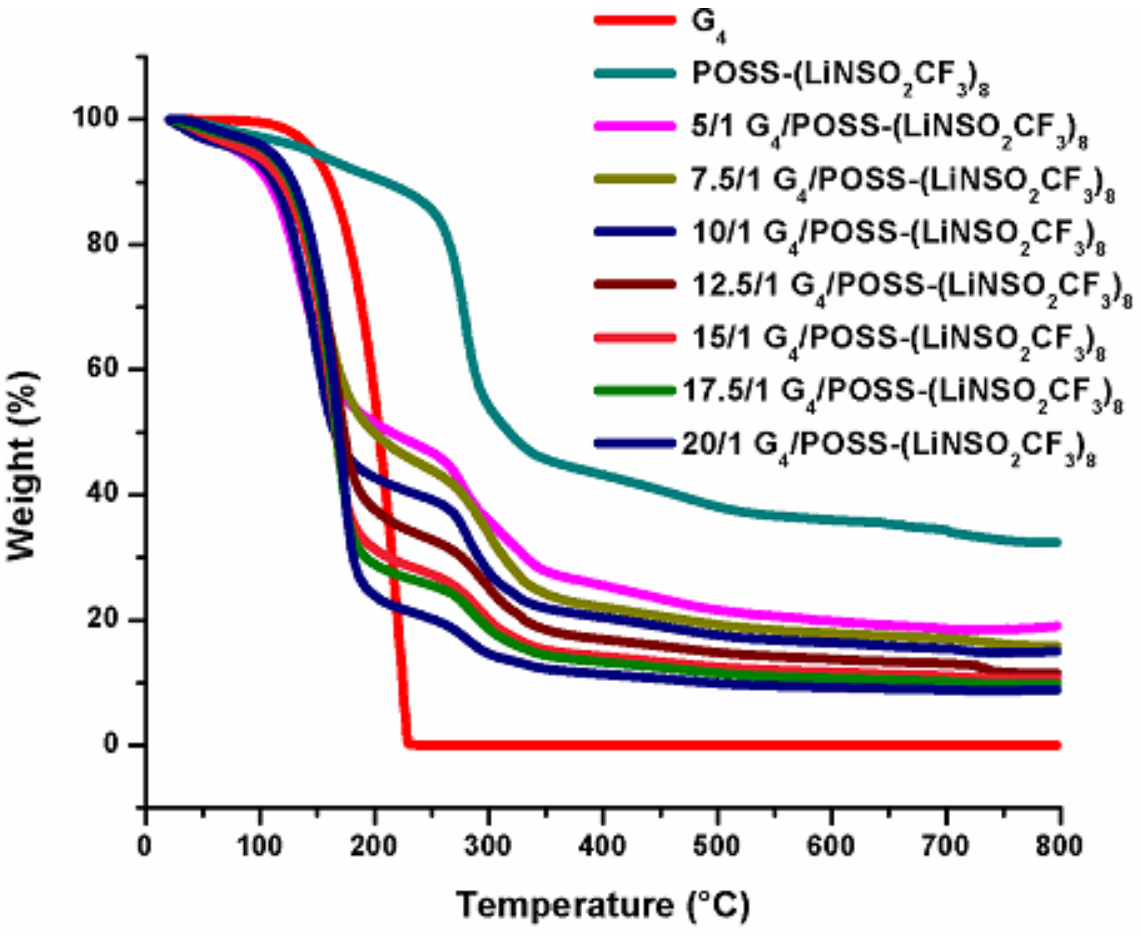

Figure S3. Thermogravimetric analysis (TGA) data for G_4 and POSS-$(LiNSO_2CF_3)_8$ and their mixtures as a function of O/Li ratio. The degradation temperature (T_d), which occurs at $T_d \sim 150\ ^0C$, is determined by T_d of G_4 (boiling point $T_b = 275\ ^0C$). Since POSS-$(LiNSO_2CF_3)_8$ has a residual mass of ~ 40 wt%, the weight loss of the mixtures decreases as the amount of POSS-$(LiNSO_2CF_3)_8$ increases.

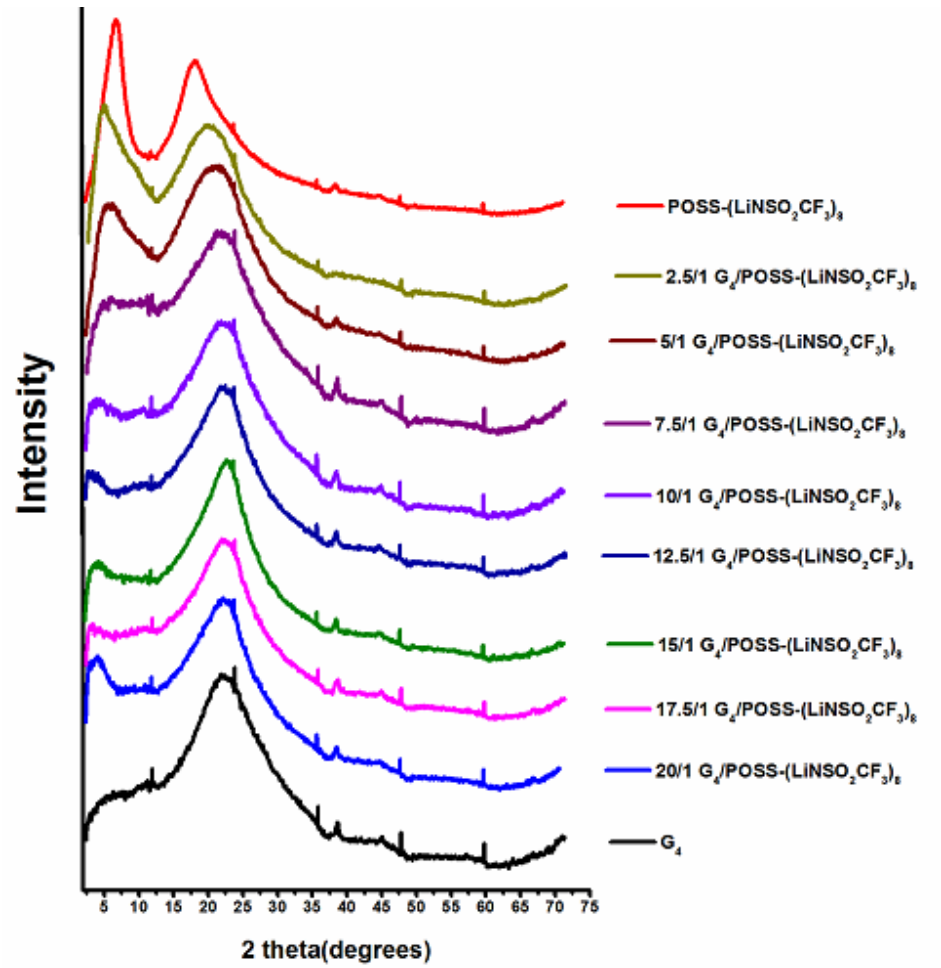

Figure S4. WAXS data for neat G_4, neat POSS-$(LiNSO_2CF_3)_8$, and mixtures of G_4/POSS-$(LiNSO_2CF_3)_8$ as a function of O/Li ratio at 25°C.

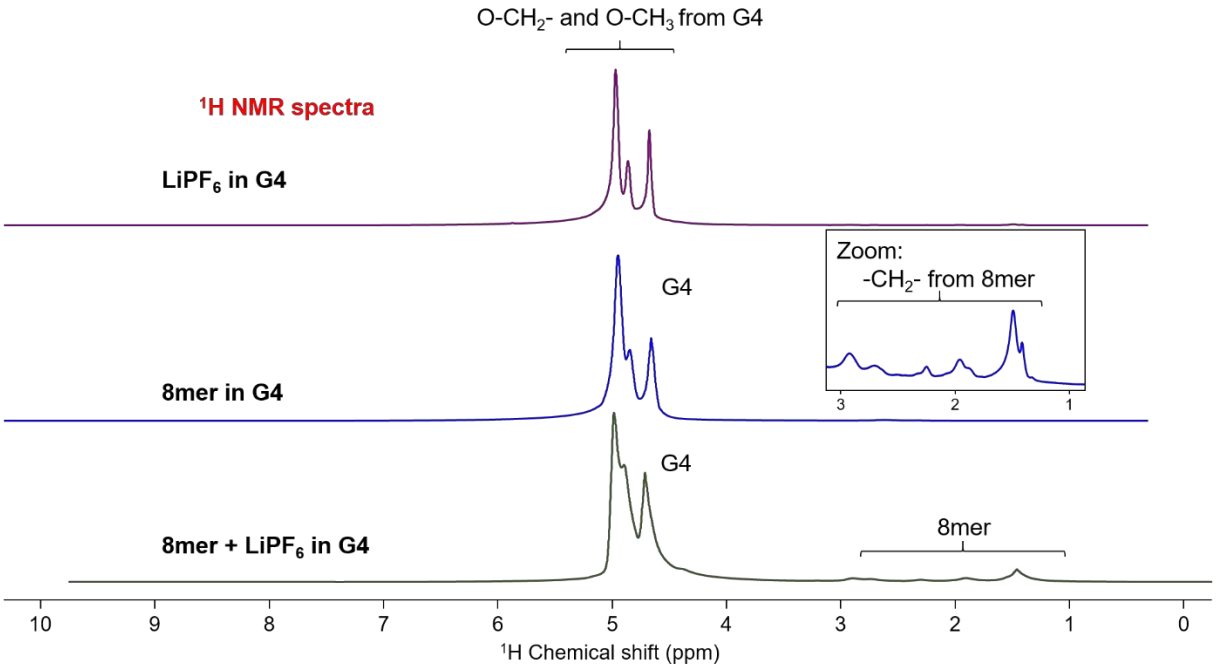

Figure S5. ^{1}H spectra of G_4/LiPF6, G_4/ POSS-$(LiNSO_2CF_3)_8$ and G_4/[80 wt% $LiPF_6$ + 20 wt% POSS-$(LiNSO_2CF_3)_8$

Electrochemical Data

Conductivity data

EIS data at low temperature consist of depressed semicircles at higher frequencies and slanted lines at lower frequencies. Data were fit using the equivalent circuit consisting of the blocking electrode capacitance in series with a parallel combination of the bulk resistance and capacitance of the electrolyte, with R_b obtained from the intercept of the slanted line extrapolated to the real axis[6]. At higher temperatures the semicircle disappears as it shifts to higher frequencies due to the increase in temperature of the electrolyte. Conductivity is calculated from = t/AR_b, where t (cm), A (cm^2), R = membrane thickness, area and resistance (Ω).

Lithium Ion Transference Number (t_{Li}^+)

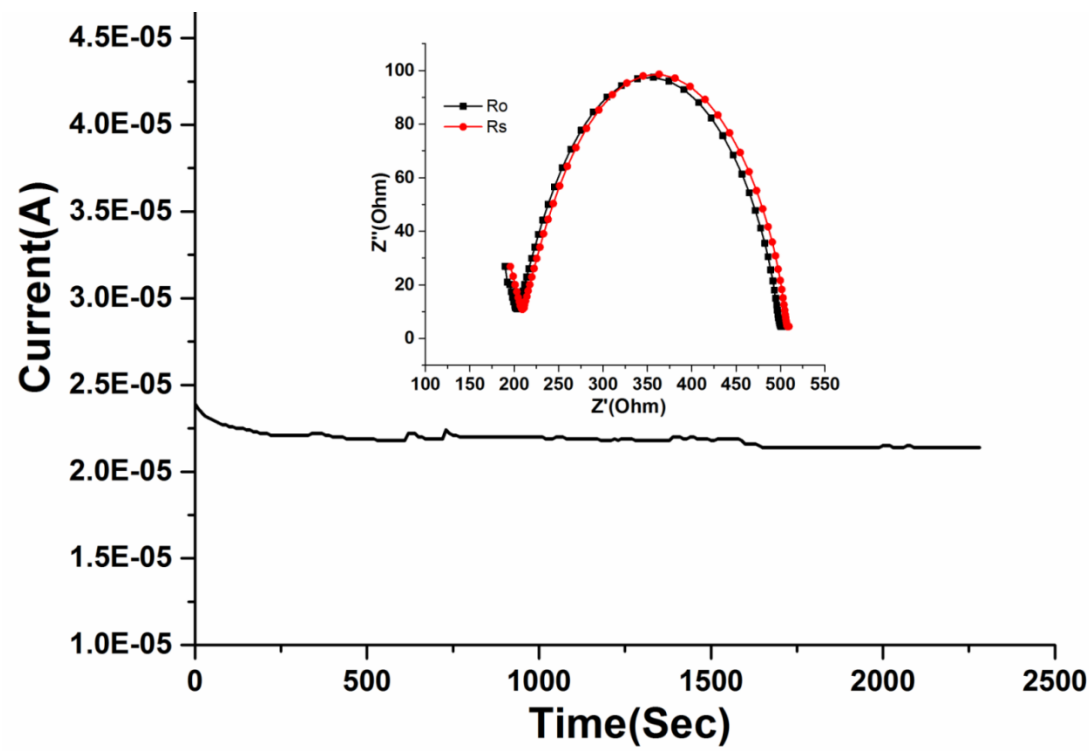

Figure S6. Current (I) versus time for $Li^0/[G_4/$ POSS-$(LiNSO_2CF_3)_8/Li^0$ cell using ΔV = 20 mV at 25 ^{0}C. Inset shows impedance (Z′′ vs Z′) of cell taken before (R_0) and after (R_s) polarization; $t_{Li}^+ = 0.65$

Linear Sweep Voltammetry

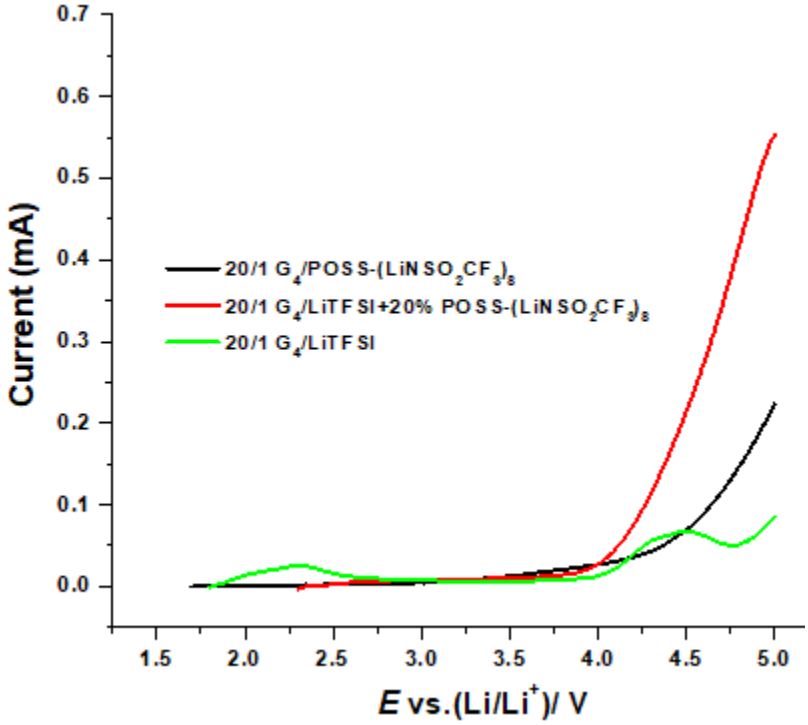

Figure S7. Anodic scans at 25 ^{0}C, 2 mV/sec from OCV to 5V, using stainless steel working electrodes, Li^{0} reference/counter electrodes, of the electrolytes (all O/Li = 20/1): (▬) G_4/POSS-$(LiNSO_2CF_3)_8$; (▬) G_4/LiTFSI; and (▬) G_4/LiTFSI+20% POSS-$(LiNSO_2CF_3)_8$ at 25°C.

Interfacial Resistance

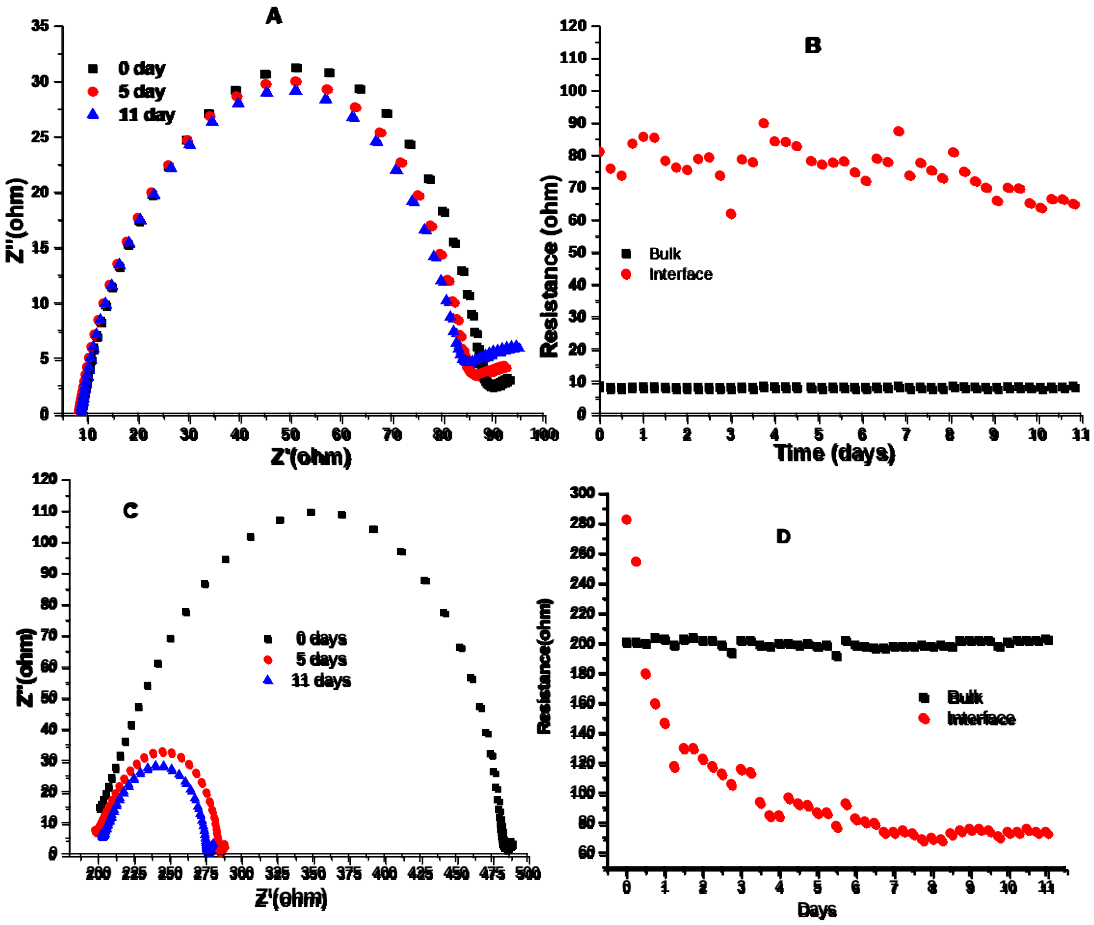

Figure S8. Time dependence under open circuit voltage (OCV) at 25°C of: (i) Li^0/[G_4+80%LiTFSI+20% POSS-$(LiNSO_2CF_3)_8$]/Li^0 (**A**) Z′′ vs Z′; (**B**) bulk and interfacial resistance; and (ii) Li^0/[G_4+ POSS-$(LiNSO_2CF_3)_8$]/Li^0 (**C**) Z′′ vs Z′; (**D**) bulk and interfacial resistance

Li^0/Li^0 Cyclng

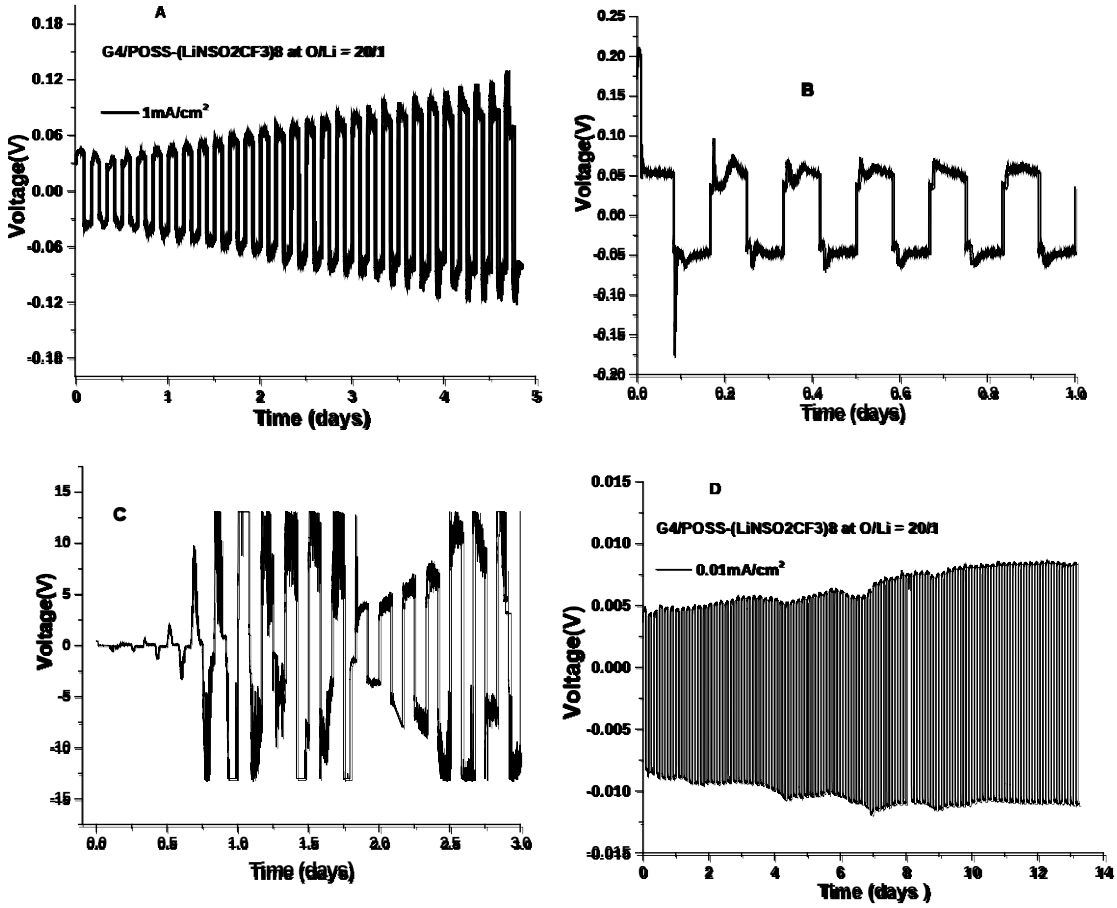

Figure S9. Li^0/electrolyte(O/Li = 20/1)/Li^0 cycling at 25 °C using 2 h charge/discharge, I = 1 mA/cm^2 for: (**A**) G_4/(80%LiTFSI+20% POSS-$(LiNSO_2CF_3)_8$; (**B**) G_4/LiTFSI; (**C**) G_4/ POSS-$(LiNSO_2CF_3)_8$; (D) G_4/POSS-$(LiNSO_2CF_3)_8$

CV Data

CV was used to study the reversibility of the Li/(G_4/POSS-($LiNSO_2CF_3$)$_8$ O/Li = 20/1)/$LiFePO_4$ system. **Figure S9** shows that at 0.1 mV/s the system is reversible (peak separation between anodic current and cathodic current is less than 58mV). At 0.2 mV/s the peak separation increases (to 60 mV), suggesting that lithium ion migration is diffusion controlled. At the higher scan rate, the peaks broaden due to the viscosity of the electrolyte and low bulk conductivity. The high resistance is probably the result of two mass-transfer mechanisms, i.e. Li diffusion in the bulk and Li diffusion through the $LiFePO_4$ particle–electrolyte interface. The peak positions at each scan rate are the same but the height of the peak decreases with cycle number.

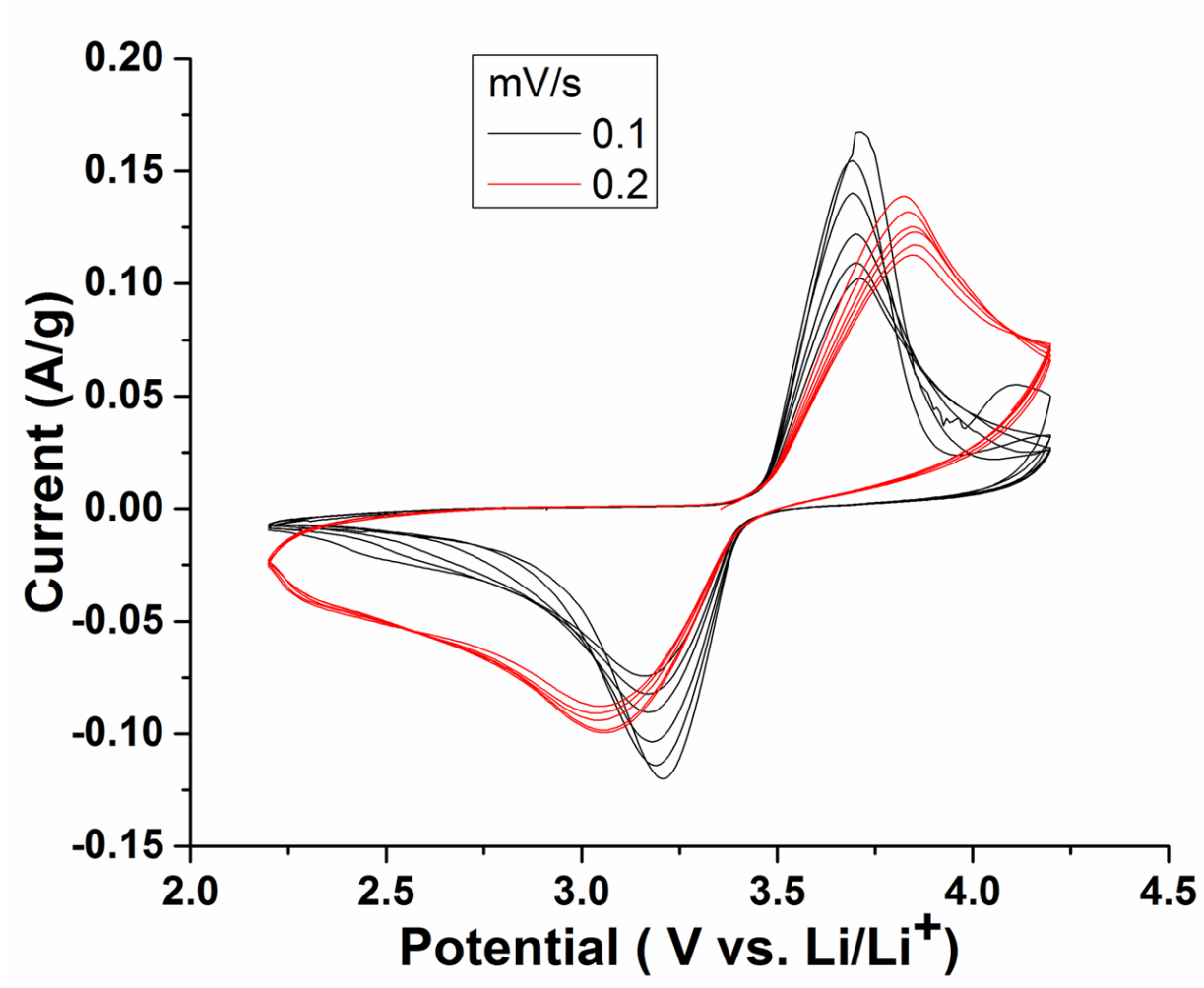

Figure S10. Cyclic voltammetry (CV) measurement for a Li^0/electrolyte/$LiFePO_4$ coin cell, where electrolyte is G_4/POSS-($LiNSO_2CF_3$)$_8$ (O/Li = 20/1), at 25°C, showing lithium intercalation and de-intercalation.

Half-Cell Cycling

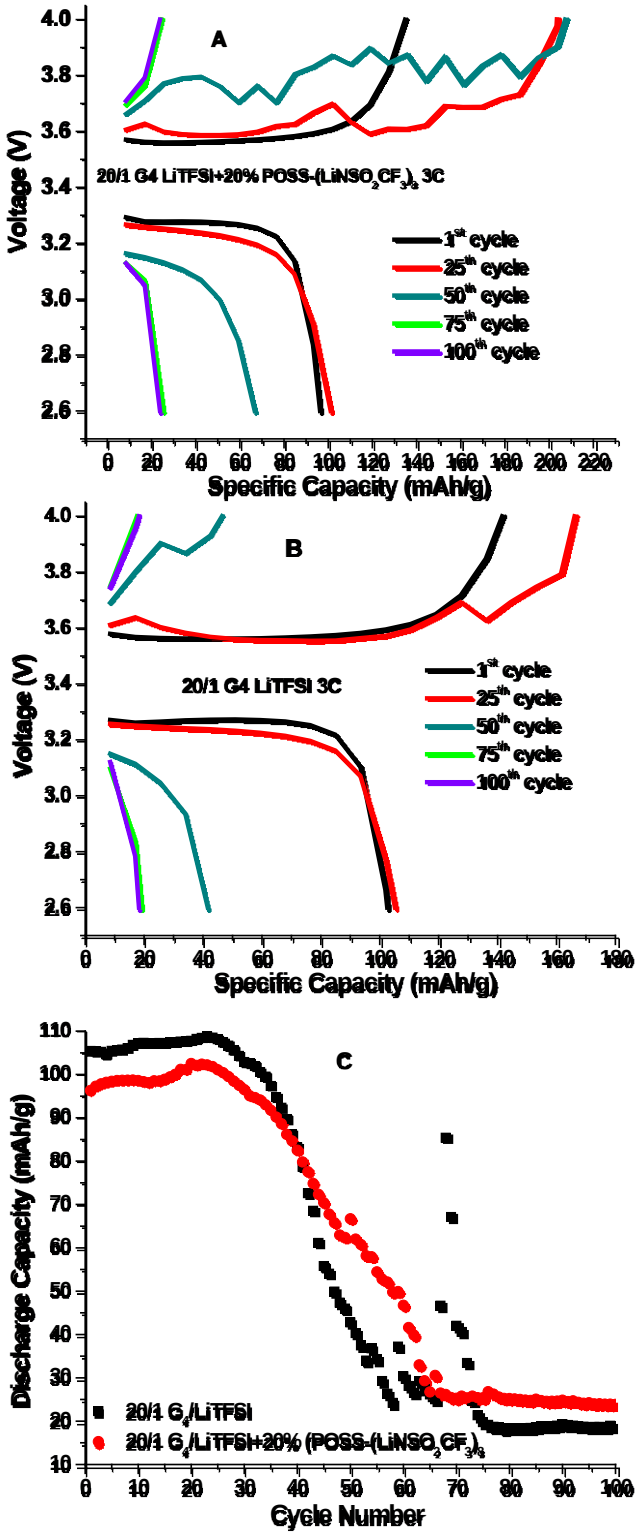

Figure S11. Cell voltage vs specific capacity profiles for Li/electrolyte (O/Li = 20/1)/$LiFePO_4$ cells at 3C rate, 25 ^{o}C using (**A**) G_4/LiTFSI+20% POSS-$(LiNSO_2CF_3)_8$; (**B**) G_4/LiTFSI; and (**C**) discharge capacity versus cycle number for **A** and **C**.

The capacity fade starts at around 30 cycles, drops until 60 cycles and then levels off, with the capacity of the cell using the 20/1 G_4/LiTFSI+20% POSS-$(LiNSO_2CF_3)_8$ electrolyte capacity dropping more slowly than that with the G_4/LiTFSI electrolyte.

References

1. Chinnam, P. R. Multi-ionic lithium salts for use in solid polymer electrolytes for lithium batteries. PhD Thesis, Temple University, Philadelphia, PA, 2015.
2. Evans, J.; Vincent, C. A.; Bruce, P. G., Electrochemical measurement of transference numbers in polymer electrolytes. *Polymer* **1987,** 28, (13), 2324-2328.
3. Bruce, P. G.; Vincent, C. A., Steady state current flow in solid binary electrolyte cells. *Journal of Electroanalytical Chemistry* **1987,** 225, (1-2), 1-17.
4. Bruce, P. G.; Evans, J.; Vincent, C. A., Conductivity and transference number measurements on polymer electrolytes. *Solid State Ionics* **1988,** 28, 918-922.
5. Yoshida, K.; Tsuchiya, M.; Tachikawa, N.; Dokko, K.; Watanabe, M., Change from Glyme Solutions to Quasi-ionic Liquids for Binary Mixtures Consisting of Lithium Bis(trifluoromethanesulfonyl)amide and Glymes. *Journal of Physical Chemistry C* **2011,** 115, (37), 18384-18394.
6. Bruce, P. G., Polymer Electrolyte Reviews. In MacCallum, J. R.; Vincent, C. A., Eds. Elsevier Applied Science: Amsterdam, 1987; Vol. 1, p 237.